metals

MDPI

Article

Effect of Segregation Band on the Microstructure and Properties of a Wind Power Steel before and after Simulated Welding

Xuelin Wang [1,2,*], Xiaoya Wang [2], Wenle Liu [1,2] and Chengjia Shang [1,3,*]

[1] Yangjiang Branch, Guangdong Laboratory for Materials Science and Technology (Yangjiang Advanced Alloys Laboratory), Yangjiang 529500, China; liuwl@yjlab.org.cn
[2] Collaborative Innovation Center of Steel Technology, University of Science and Technology Beijing, Beijing 100083, China; wangxiaoyahy@163.com
[3] State Key Laboratory for Advanced Metals and Materials, University of Science and Technology Beijing, Beijing 100083, China
* Correspondence: xuelin2076@ustb.edu.cn (X.W.); cjshang@ustb.edu.cn (C.S.)

Abstract: This article uses scanning electron microscopy (SEM) and electron back-scattering diffraction (EBSD) to study the effect of C and Mn segregation on the microstructure and mechanical properties of high-strength steel with 20 mm thickness used for wind power before and after simulated welding. A Gleeble-3500 (GTC, Dynamic Systems Inc., Poestenkill, NY, USA) was used to study the microstructure evolution of the simulated coarse-grained heat-affected zone (CGHAZ) of experimental steel under different welding heat inputs (10, 14, 20, 30 and 50 kJ/cm) and its relationship with low-temperature impact toughness (−60 °C). The results indicate that alloy element segregation, especially Mn segregation, significantly affects the impact toughness scatter of the steel matrix, as it induces the formation of low-temperature martensite or hard phase, such as M/A (martensite/austenite) constituent. In addition, segregation also reduces the low-temperature impact toughness of the simulated welding samples and increases the fluctuation range. For high-strength steel with yield strength higher than 460 MPa used for wind power generation, there is an optimal welding heat input (~20 kJ/cm), which enables the simulated coarse-grained heat-affected zone (CGHAZ) to obtain the highest impact toughness due to the formation of lath bainite (LB) and the finest crystallographic block units. Excessive or insufficient heat input can induce the formation of coarse granular bainite (GB) or lath martensite (LM), leading to a larger size of crystallographic block units, reducing the hindering effect of brittle crack propagation and deteriorating low-temperature impact toughness.

Keywords: wind power; high-strength steel; segregation; simulated welding; impact toughness; crack propagation

Citation: Wang, X.; Wang, X.; Liu, W.; Shang, C. Effect of Segregation Band on the Microstructure and Properties of a Wind Power Steel before and after Simulated Welding. *Metals* **2024**, *14*, 129. https://doi.org/10.3390/met14010129

Academic Editor: Abhay Sharma

Received: 19 December 2023
Revised: 3 January 2024
Accepted: 19 January 2024
Published: 22 January 2024

1. Introduction

As a kind of clean energy, wind energy has great potential for future development. And with the rapid development of wind power generation, the tubular steel tower used as the supporting structure is becoming increasingly large [1]. In order to ensure the safety of the entire tower, advanced steel materials with higher strength have been developed and applied. The steel used for onshore wind tubular steel towers has developed from 355 MPa to 420 and 460 MPa levels, which can decrease the material and transportation costs, thus increasing its market competitiveness [2]. As we all know, the tower is mainly made of medium-thick plate curling and welding, so the problems faced by high-strength wind power steel have shifted from the base plate to the weld joint. The excellent balance of high strength and toughness in the base plate will be upset by the welding thermal cycles characterized by rapid heating and a variable cooling rate with high peak temperature [3,4]. Among them, the coarse-grained heat-affected zone (CGHAZ) is the region always showing the worst toughness because of the formation of coarse austenite grains and undesirable

microstructure [5–7]. Previous studies [4,8–12] have extensively investigated the effects of welding heat input, cooling rate, alloy composition, post-weld heat treatment and other parameters on the microstructure and properties of the weld joint. However, a recent study [13] has also found that segregation in steel plates can also affect the microstructure and mechanical properties of high-strength steel before and after welding. From this, it can be seen that in addition to welding process parameters, the metallurgical quality of the steel plate is also crucial.

Previous studies [14–17] have shown that as the degree of centerline segregation in steel plates increases, the strength and low-temperature impact toughness significantly deteriorate, and the hydrogen embrittlement sensitivity is significantly improved. This is because the segregation of alloy components, such as C, Mn and Si, induces the formation of the hard second phase of martensite. From the view of crystallographic features, the severe segregated zone with high-level enrichment of alloying elements produced a large packet or Bain zone size due to strong variant selection, which was unfavorable for crack deflection or arrest [15]. In addition, research [13] has also found that the segregation yielded in base metal can be inherited into the weld joint, resulting in adverse effects on the microstructure and properties of the heat-affected zone (HAZ). The microstructure obtained in the segregation zone of the base metal will undergo re-austenitization under the influence of the welding thermal cycle and then transform into a hard martensitic structure during the cooling process, causing the increase in the local stress and hardness. The mismatch between the hard phase and the surrounding normal structures leads to a sharp decrease in the low-temperature toughness of the weld joint. Another study [18] also found that segregation can induce the formation of coarse MnS or other inclusions at the core of the steel plate, which can easily become the source of crack initiation and significantly deteriorate the mechanical properties and low-temperature toughness of the steel plate before and after welding. However, there is still a lack of research on the effect of segregation on the microstructure and properties of the new generation of high-strength steel used for wind power before and after welding. This article aims to study the evolution of microstructure and properties of the surface and core in a wind power steel plate with a yield strength of 460 MPa, as well as the mechanism of segregation influence on the microstructure and low-temperature impact toughness of weld joints, providing theoretical and experimental bases for the development of wind power steel with high strength and good impact toughness. In addition, the visualization method of microstructure has been adopted to elucidate the relationship between brittle crack propagation paths and crystallographic structural units, such as blocks [19,20], and to clarify the mechanisms that hinder crack propagation.

2. Materials and Methods

The material used in this study was a high-strength wind power steel with thickness of 20 mm and made by thermo-mechanical controlled processing (TMCP). Due to the higher strength of the steel plate used in this study compared to traditional 355 MPa wind power steel, and mainly used for onshore wind power, the thickness specification (20–40 mm) is smaller than 355 MPa wind power steel (40–70 mm). The chemical composition is shown in Table 1. In order to study the effect of segregation bands on the microstructure and properties of steel plates before and after welding, welding simulated samples were taken from the surface and 1/2 core positions of the steel plate, and welding simulated experiments with different heat inputs (10, 14, 20, 30 and 50 kJ/cm) were completed on a Gleeble-3500 (GTC, Dynamic Systems Inc., Poestenkill, NY, USA) with an average heating rate of 130 °C/s and a peak temperature of 1300 °C. After thermal simulation, standard impact specimens with the size of 10 mm × 10 mm × 55 mm were prepared to evaluate Charpy V-Notch (CVN) impact toughness at −60 °C. For impact samples, the sampling method was to take samples along the rolling direction (RD) and at the near-surface and 1/2 core positions on the side of the steel plate, while the V-shaped direction is parallel to the normal direction (ND) of the steel plate. Meanwhile, tensile properties of the surface

and core of the base metal were measured at room temperature using standard tensile samples machined to 5 mm diameter and 25 mm gauge length according to the ASTM E8 specification [21]. The sampling direction of the tensile sample is along the transverse direction (TD). And the impact toughness of the base metal was also measured at different temperatures using the standard Charpy V-notch (CVN) test. In addition, three standard impact samples and two standard plate-shaped tensile samples were used to obtain the average values of low-temperature toughness and strength. Hardness evolution from the normal zone to segregation band was measured with 100 gf and a dwell time of 15 s, according to ASTM: E384 [22]. And the hardness testing experiment was completed under room-temperature conditions.

Table 1. Chemical composition of the studied steel (wt.%).

C	Si	Mn	P	S	Cr	Ni	Nb	Ti
0.10	0.22	1.64	0.008	0.002	0.35	0.17	0.002	0.019

For the characterization of microstructure, the samples were cut from the heat-treated and untreated areas of the impact fracture specimens and then were mounted, mechanically polished and etched with 4% nital for optical microscopy (OM) and scanning electron microscopy (SEM) observation firstly. Fracture surfaces of the samples after Charpy impact tests were also characterized by SEM. To obtain the crystallographic information of transformation structure, electron back-scattering diffraction (EBSD) analysis was carried out after mechanical and electrolytic polishing using TESCAN CLARA field emission SEM (TESCAN, Brno, Czech) at an acceleration voltage of 20 kV. HKL Channel 5 software from Oxford-HKL (6.1, Oxford Instruments, Abingdon, UK) was also employed for post-processing orientation data. Meanwhile, for the identification of the segregation band, electron probe microanalysis (EPMA) experiments were performed to inspect the chemical composition. Additionally, the correlation between crystallographic structure and crack propagation behavior in the simulated CGHAZ was analyzed by using EBSD, aiming to reveal the mechanism of microstructure in preventing brittle cracks.

3. Results

3.1. Tensile Properties and Impact Toughness of Base Metal

Figure 1 shows the strength and low-temperature impact toughness test results of the surface and core of the steel plate, respectively. It can be observed that the yield strength of the surface and core reaches 464 and 502 MPa, respectively, which is opposite to the result of lower strength obtained in the core of traditional thick plate [23]. From the impact toughness test results, it can be found that even if the test temperature is reduced to −80 °C, the impact toughness of the surface and core can still reach over 100 J, which is far higher than the minimum standard requirement of 460 MPa grade low-alloy steel (national standard GB/T 1591-2018 [24]: 16 and 27 J correspond to the minimum requirements of transverse and longitudinal directions at −60 °C). This indicates that the experimental steel has excellent comprehensive properties. However, although the average values of impact toughness obtained at various temperatures on the surface and core are basically the same, the larger scatter in impact toughness occurred in the sample of core. From these, it can be preliminarily determined that the difference in strength and the scatter in impact toughness are inevitably related to the differences in microstructure.

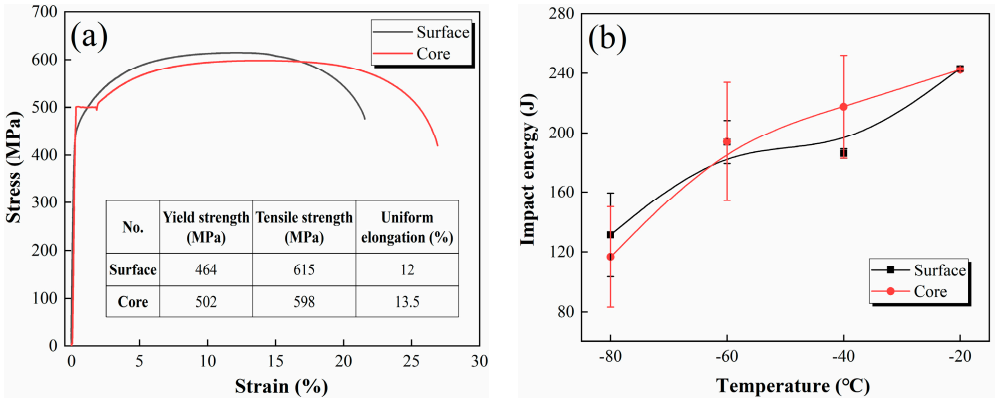

Figure 1. Engineering stress–strain curves (**a**) and low-temperature impact toughness (**b**) evolution in the steel of surface and core.

3.2. Microstructure Evolution in Base Metal

Figure 2 shows the microstructure obtained at the surface and core of the steel plate using OM and SEM. It can be found that the experimental steel is composed of typical polygonal ferrite and pearlite, and the volume fraction of ferrite obtained at the surface is ~88% (Figure 2a–c). Meanwhile, the sample of core presents a typical segregation band, which is composed of martensite and M/A (martensite/austenite) constituent (Figure 2d–f). This is also the reason why the yield strength of the core is slightly higher than the surface. In addition, the greater variability of low-temperature impact toughness in the core is closely related to the formation of martensite. When the sampling location includes a higher proportion of martensite, the low-temperature impact toughness is lower, and vice versa, it is higher. Apparently, this is due to the severe segregation of alloying elements, which improves the hardenability, reduces the critical cooling rate of the core region, and promotes the occurrence of martensitic transformation [25]. To verify this mechanism, EPMA and hardness testing were used to demonstrate the segregation of alloy components and the high hardness of the phase transformation structure, as shown in Figure 3. The hardness of the microstructure in the segregation band reaches 321.2 HV, which is significantly higher than that of normal microstructure by ~220 HV, further confirming the high tendency of martensitic structure. Moreover, the area scanning and line scanning results of the alloy composition by EPMA showed significant enrichment of C and Mn, with the highest level of 0.7 and 3.0 wt.%, respectively, and significantly higher than the average concentration of the matrix (Table 1).

Previous studies [14,15] have shown that the more severe the central segregation, the lower the low-temperature impact toughness of the steel plate and the higher the ductile–brittle transition temperature (DBTT). If the enrichment of C and Mn is too high, it can still induce the formation of low-temperature bainite or martensite even at lower undercooling. However, the segregation inherited from the continuous casting process is difficult to optimize through subsequent heat treatment, but the latest study [26] shows that using a two-step intercritical heat treatment method can tailor the microstructure of the segregation band and improve the low-temperature toughness and ductility by promoting the formation of retained austenite. The formation of centerline segregation in the studied steel did not significantly reduce its mechanical properties and low-temperature impact toughness, but increased the scatter of impact toughness. Further discussion will be conducted on whether the segregation affects the welding performance.

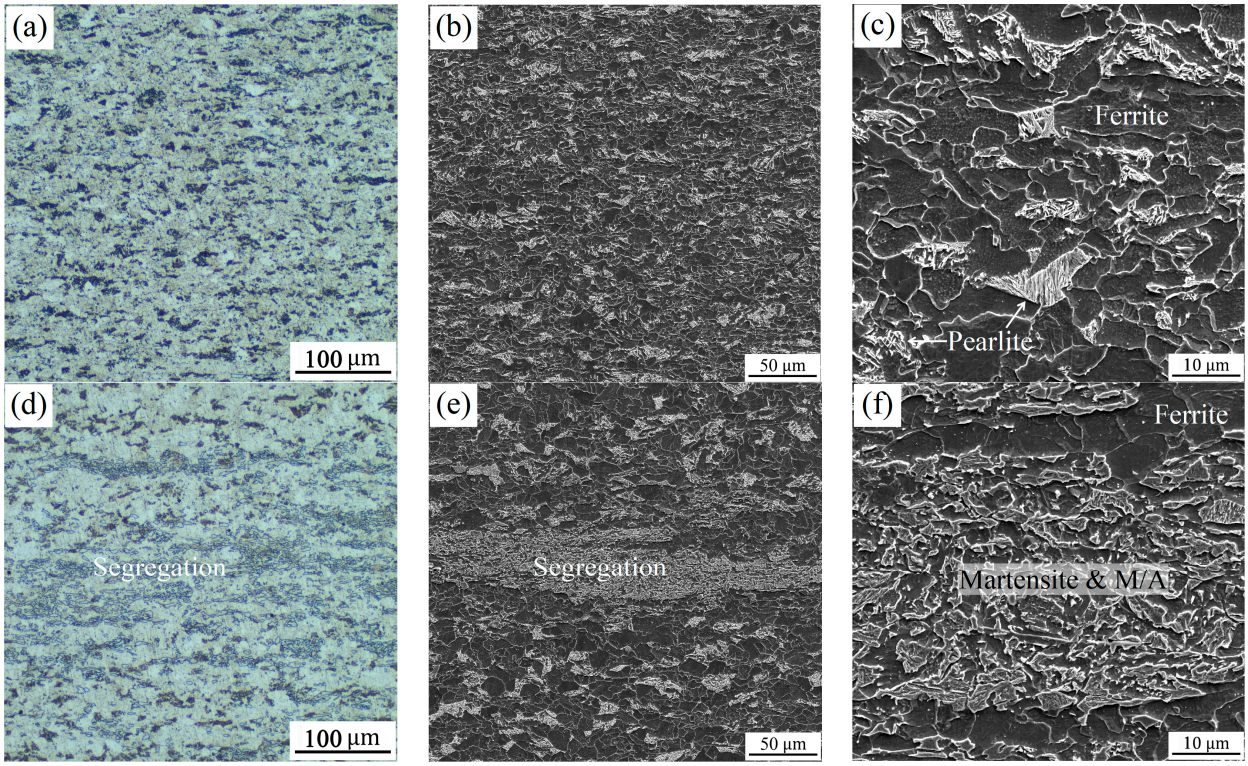

Figure 2. OM (**a**,**d**) and SEM (**b**,**c**,**e**,**f**) showing the microstructure obtained in the studied steel of surface (**a**–**c**) and core (**d**–**f**).

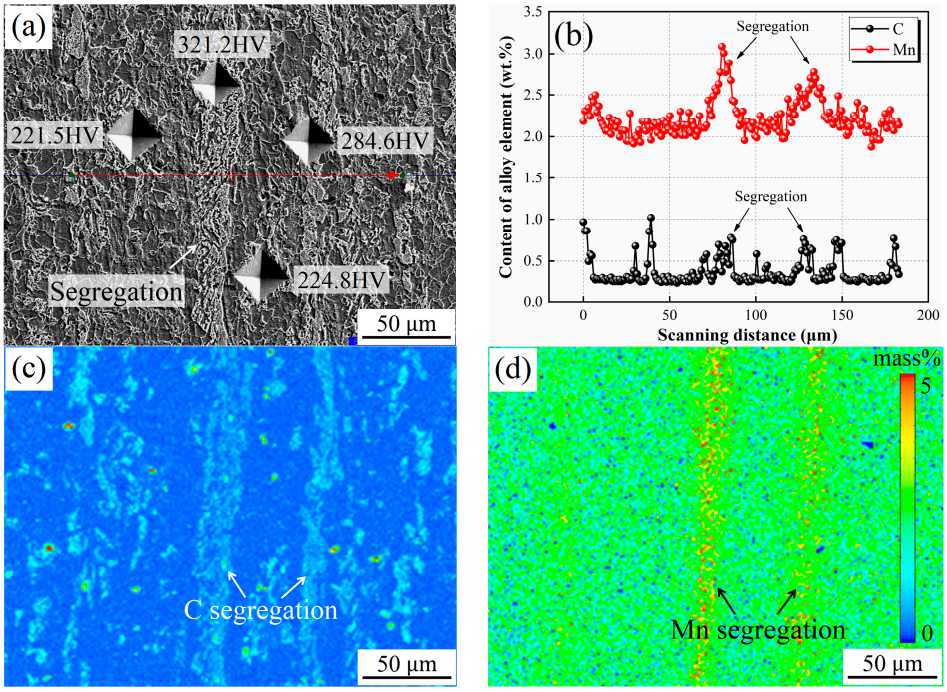

Figure 3. Hardness (**a**) and composition (**b**–**d**) testing results of the segregation zone obtained from the sample of core: (**b**–**d**) line and area scanning by using EPMA.

3.3. Impact Toughness and Fractographs of Thermal Simulated Samples

The variation of the impact toughness of the surface and core after CGHAZ simulation under different heat inputs is shown in Figure 4. It can be clearly seen that the impact toughness of the surface and core show a similar trend of first increasing and then de-

creasing with the increase in heat input, and reaches its peak at 20 kJ/cm. It indicates that there is an optimum window of heat input for the welding of the studied steel, which is consistent with the previous study on ultra-high-strength steel [27,28]. Excessive heat input can lead to a sharp deterioration of impact toughness, while insufficient heat input can significantly reduce welding efficiency, although the degree of low-temperature impact toughness deterioration is relatively low. This can also be confirmed by the observation of impact fracture morphology, as shown in Figures 5 and 6.

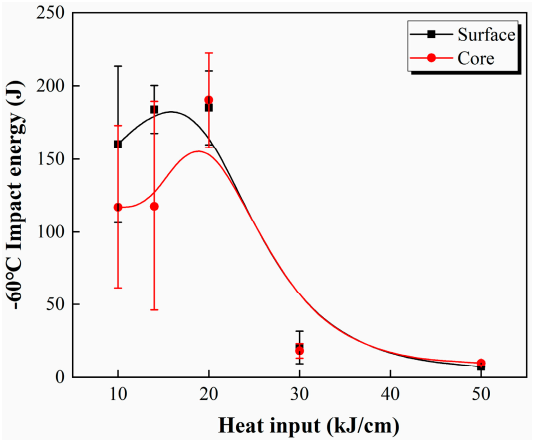

Figure 4. Charpy impact toughness of the welding simulated samples obtained from the steel of surface and core.

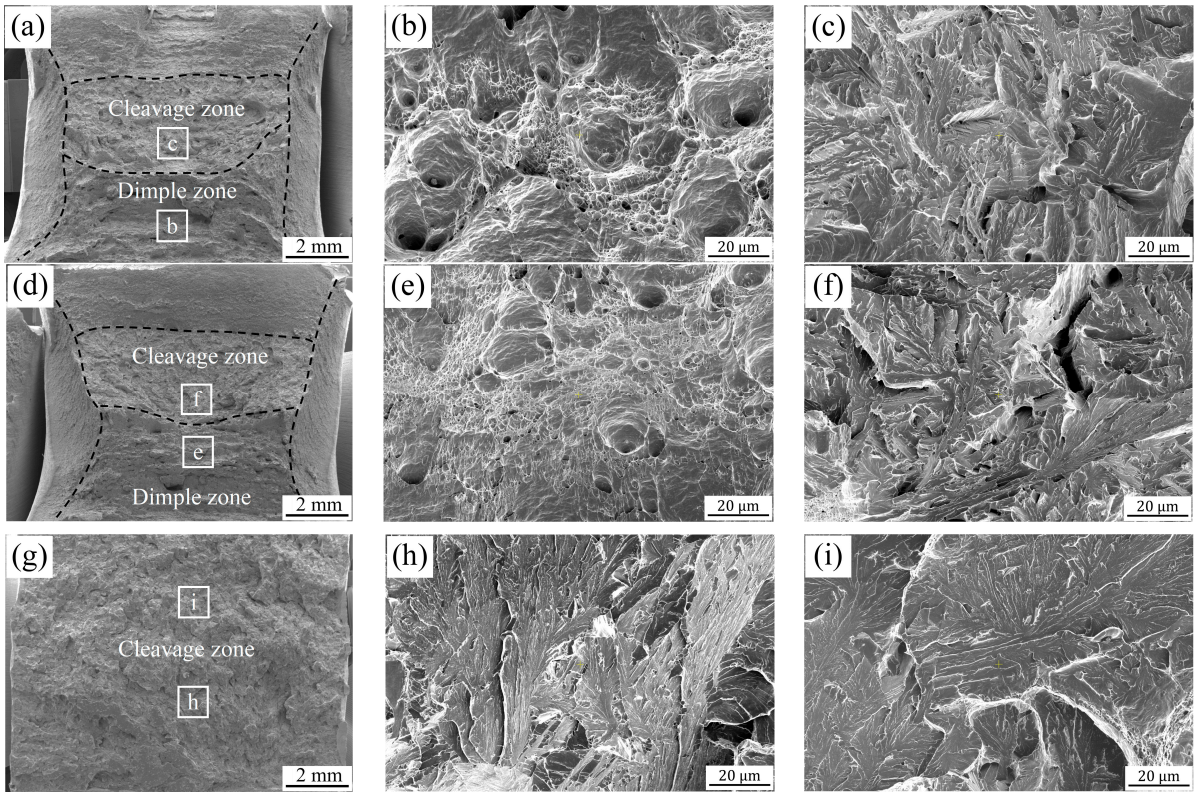

Figure 5. SEM micrographs showing the fracture surface after Charpy impact tests for the simulated samples of surface with heat input of 10 kJ/cm (**a**–**c**), 20 kJ/cm (**d**–**f**) and 30 kJ/cm (**g**–**i**).

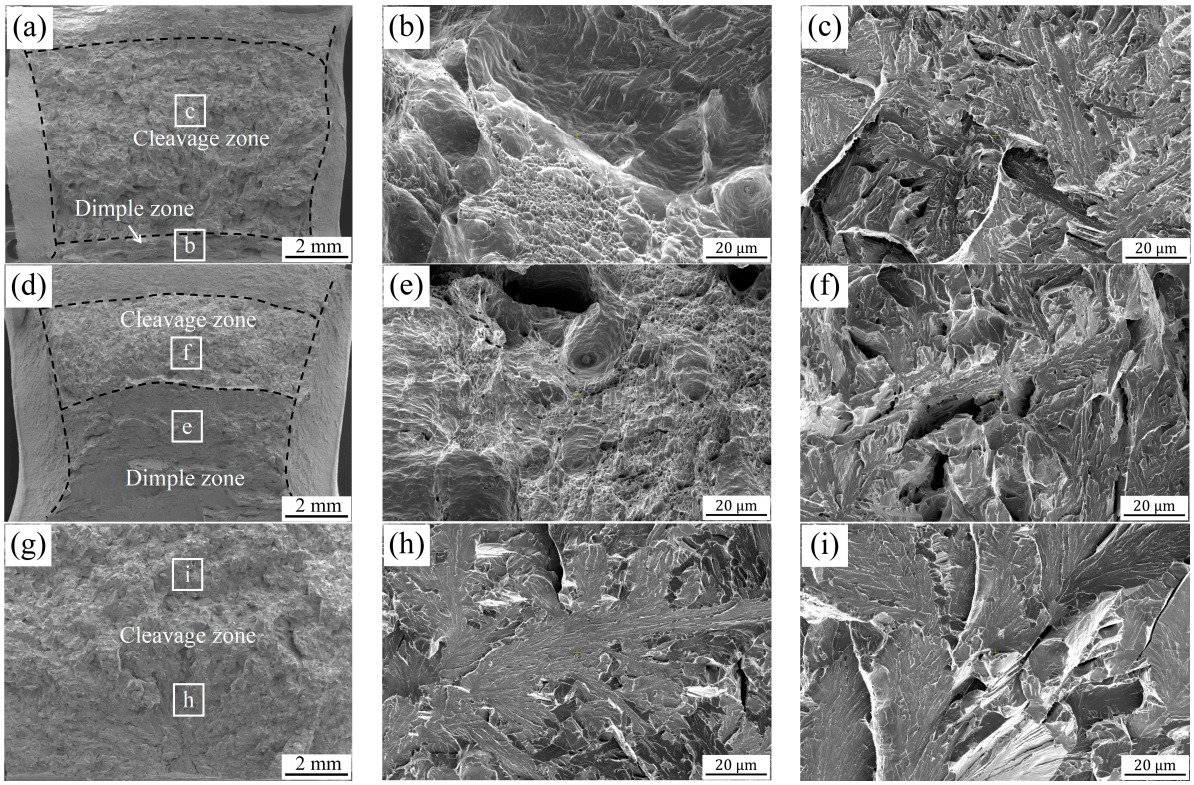

Figure 6. SEM micrographs showing the fracture surface after Charpy impact tests for the simulated samples of core with heat input of 10 kJ/cm (**a**–**c**), 20 kJ/cm (**d**–**f**) and 30 kJ/cm (**g**–**i**).

Under heat inputs of 10 and 20 kJ/cm, the fracture surface exhibits ductile and brittle fracture characteristics, with a distribution of dimple and cleavage patterns (Figures 5a,d and 6a,d). As the heat input increases to 30 kJ/cm, the complete cleavage fracture morphology is presented (Figures 5g and 6g). It can also be observed that with the increase in heat input, the area fraction of cleavage fracture first decreases and then increases, which is consistent with the trend of change in impact toughness (Figure 4). Furthermore, it was found that under a heat input of 10 kJ/cm, the area of the cleavage fracture in the core (Figure 6a) was significantly larger than that on the surface (Figure 5a), indicating lower impact toughness. Of course, this is also closely related to the large scatter of impact toughness value obtained in the simulated CGHAZ of the core (Figure 4), and is likely due to the influence of centerline segregation. Therefore, in order to further elucidate the influence of segregation on the impact toughness of welding simulation samples, hardness testing and composition calibration were carried out on the segregation zone of the simulated HAZ using a hardness tester and EPMA, respectively, as shown in Figure 7.

From the impact fracture of the sample subjected to thermal simulation at a heat input of 20 kJ/cm, it can be clearly observed that the segregation band is formed in the core of the steel plate, and the thermal cycling process does not eliminate the segregation band, as shown in Figure 7a. Figure 7b shows the OM image of the microstructure obtained in the matrix of the core corresponding to Figure 3. From Figure 7c, it can be seen that although the morphology of the segregation band in HAZ is not as clear as that of the matrix, hardness testing shows that the hardness value of the segregated structure is still higher than that of the surrounding normal structures. Combined with the results of alloy composition calibration, it can be found that the enrichment of Mn is still very serious (Figure 7f), but the enrichment of C is not significant (Figure 7e), which should be related to the high diffusion rate and low content. Nevertheless, it can be concluded that the matrix segregation of the steel plate affects the performance of HAZ. Especially, the high hardness caused by segregation can lead to local stress concentration in the weld joint,

thereby deteriorating impact toughness and other possible service performance, including the scatter of impact toughness, as shown in Figure 4.

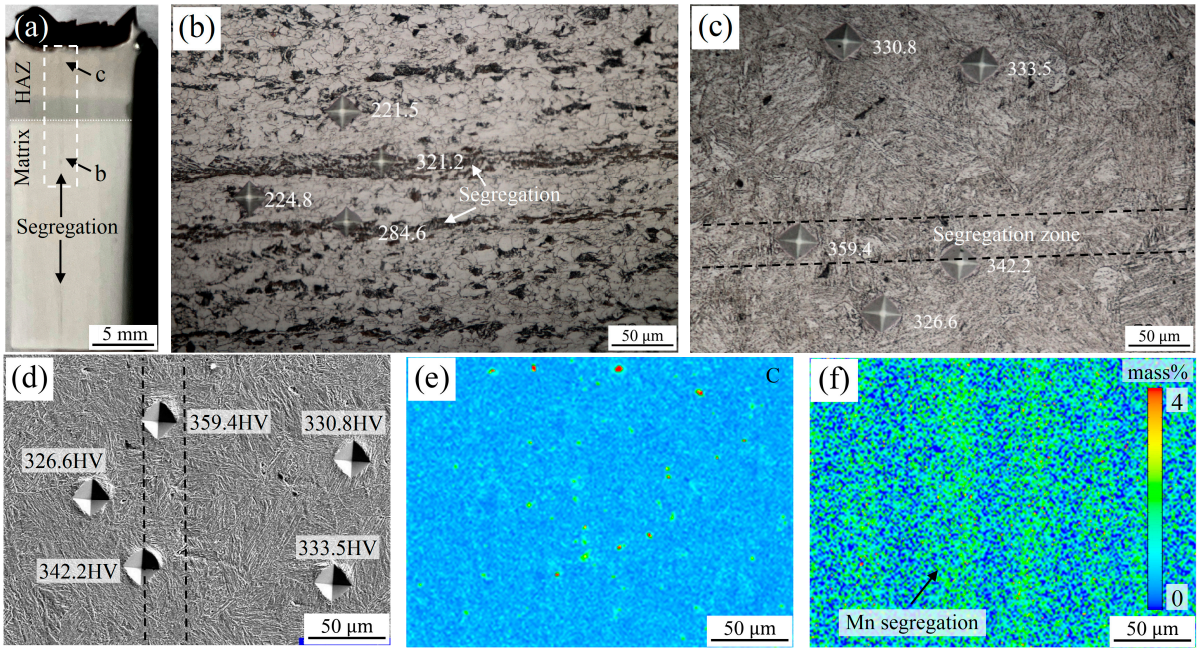

Figure 7. Analysis of segregation behavior of impact sample from the studied steel of core, which was subjected to thermal cycling at heat input of 20 kJ/cm: (**a**) segregation morphology on the impact sample; (**b**) segregation zone of the matrix corresponding to Figure 2a; (**c**) segregation zone of HAZ and hardness testing results; (**d**–**f**) segregation zone of the heat-affected zone corresponding to Figure 5c, which was rotated clockwise by 90°.

3.4. Microstructure Evolution in Thermal Simulated Samples and Phase Transformation Mechanism

Displayed in Figure 8 are the typical microstructures of the simulated CGHAZ with heat input of 10, 20 and 30 kJ/cm, which present the characteristic of martensitic and bainitic structures, i.e., lath martensite (LM), lath bainite (LB) and granular bainite (GB). Under the heat input of 10 kJ/cm, the microstructure is mainly composed of LM and LB, and the tendency of LM formation in the sample of core is higher, which is attributed to the lower phase transition temperature induced by the enrichment of C and Mn. Furthermore, as the heat input increases to 20 and 30 kJ/cm, the microstructure gradually changes into a full LB structure and a mixed structure of LB and GB, where fine carbides and coarse M/A constituents can be clearly seen, respectively. The evolution of microstructure with increasing heat input is closely related to the phase transition temperature. An increase in heat input will reduce the $t_{8/5}$ cooling rate and increase the phase transition temperature [4,27,29], which leads to a trend of microstructure transformation from LM to LB and GB. The change in microstructure is the fundamental factor determining the low-temperature impact toughness variation in Figure 4.

From Figure 8, it can be seen that the microstructure of the surface and core after thermal cycling shows a similar trend with the change of heat input. Therefore, in order to further elucidate the influence of heat input on the phase transformation mechanism and impact toughness, the crystallographic analysis method was used to reconstruct typical austenite grains obtained in the simulated CGHAZ samples of core and visualize their crystallographic features, as shown in Figure 9. At a heat input of 10 kJ/cm, the microstructure obtained in the single austenite grain exhibits a mixture of LM and LB, which can be verified from the grain boundary map, block map and KAM (Kernel average misorientation) map. According to previous studies [30,31], the LM structure is mainly dominated by the variant pairs with a small misorientation angle (such as V1/V4 and

V1/V8), and the block units are significantly larger than the LB structure. In addition, it can be clearly seen from the KAM map that the value of LM structure is significantly higher than that of LB, attributed to its higher dislocation density and phase transition stress, which can also be concluded from Figure 10b. For the LB structure obtained at the heat input of 10 and 20 kJ/cm, due to the weakest variant selection, all 24 variants that conform to the K-S (Kurdjumov–Sachs) relationship are formed in a single austenite grain, especially the block boundaries composed of a V1/V2 variant pair with a large misorientation angle, which can achieve effective refinement of austenite grains through interactive arrangement and thus play the strongest hindering role in the propagation of brittle cracks [20,32–35]. However, for the GB structure obtained at the heat input of 30 kJ/cm, the higher heat input leads to a significant increase in its phase transition temperature [29]. The bainitic variant selection is strengthened, and the coarse Bain group dominates the entire austenite grain, making it difficult to achieve the obstruction of crack propagation due to the large block units. This can also be confirmed by the relationship between the propagation path of secondary cracks on the impact fracture surface and the crystallographic structure, as shown in Figure 11.

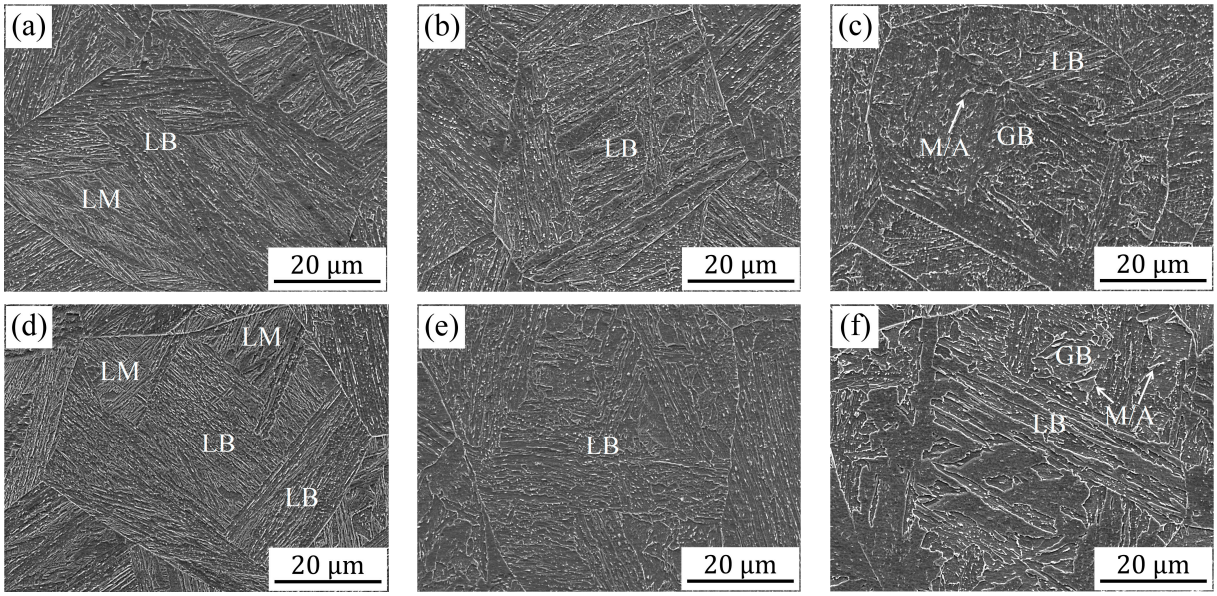

Figure 8. SEM images showing the microstructure of the simulated samples of surface (**a**–**c**) and core (**d**–**f**) with heat input of 10 kJ/cm (**a**,**d**), 20 kJ/cm (**b**,**e**) and 30 kJ/cm (**c**,**f**).

Many secondary cracks appear on the cleavage fracture surface dominated by GB structure, and the cleavage unit size is coarse, while the secondary cracks are relatively straight (Figure 11a). This is consistent with the secondary crack morphology observed in the microstructure (Figure 11b–f). Secondary cracks only deflect or arrest when encountering different block boundaries during propagation. However, Figure 11e shows that the secondary crack can propagate through different block boundaries at a smaller deflection angle during the initial propagation process, as indicated by the green arrows. From Figure 11f, it can also be seen that there is no significant plastic deformation around the propagation path of such secondary cracks, indicating that the fracture facet corresponding to the crack is cleavage fracture rather than dimple. Nevertheless, this crack was ultimately arrested at the block boundary (Figure 11e). Previous studies [20,29,36,37] have shown that the block unit is beneficial for both strength and toughness, as the misorientation angle of its boundary is greater than 45°, which can effectively hinder crack propagation. From Figure 10a, it can also be seen that the LB structure obtained at a heat input of 20 kJ/cm has the highest density of the high-angle grain boundary, which is consistent with the previous study [4]. That is, the optimal variant selection that occurs in the bainite structure

is obtained near the nose temperature of bainite transformation, with the best refinement effect of crystallographic structural units and comprehensive performance.

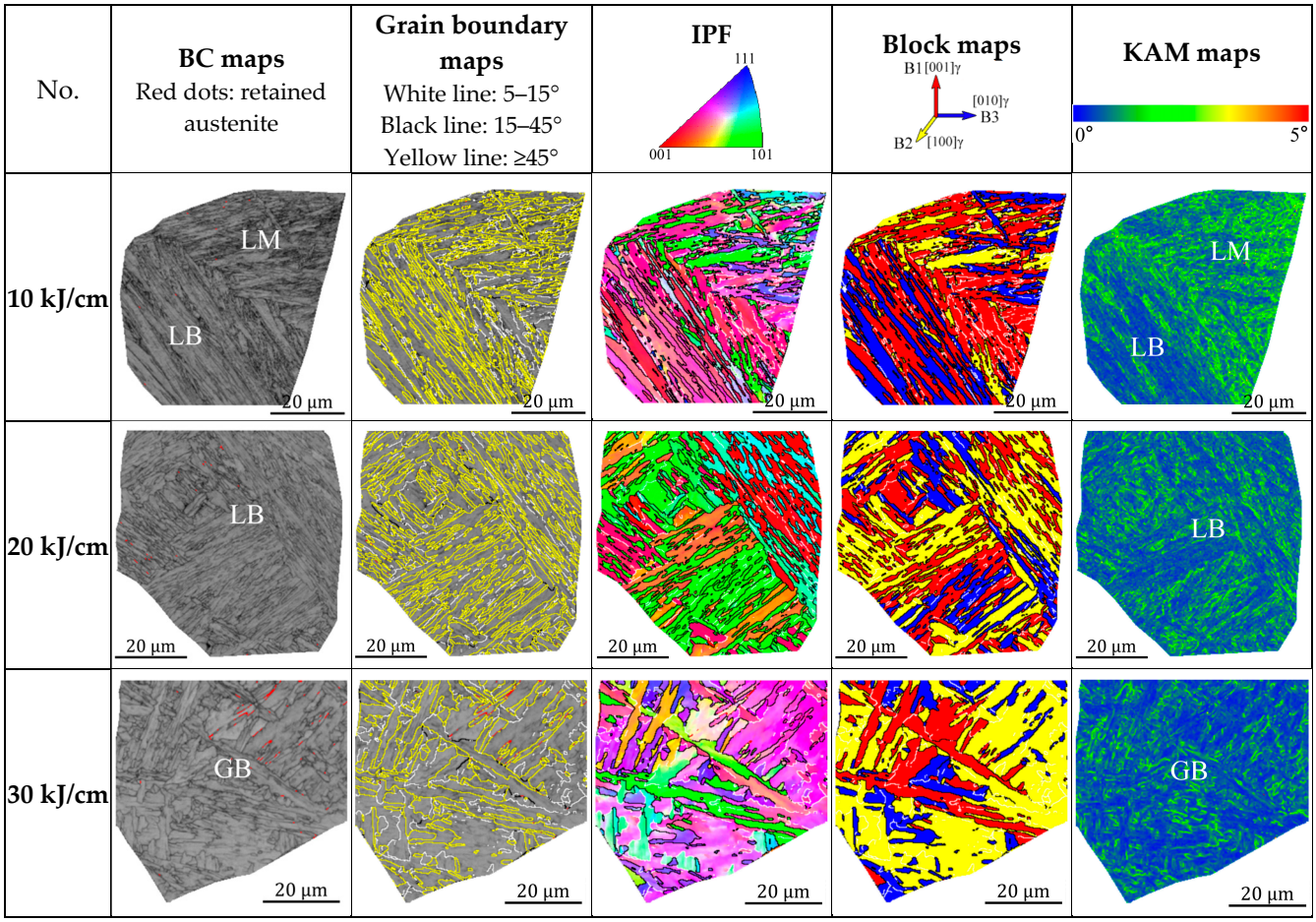

Figure 9. Reconstruction of the typical austenite grain obtained from the simulated samples of core and the corresponding crystallographic structures.

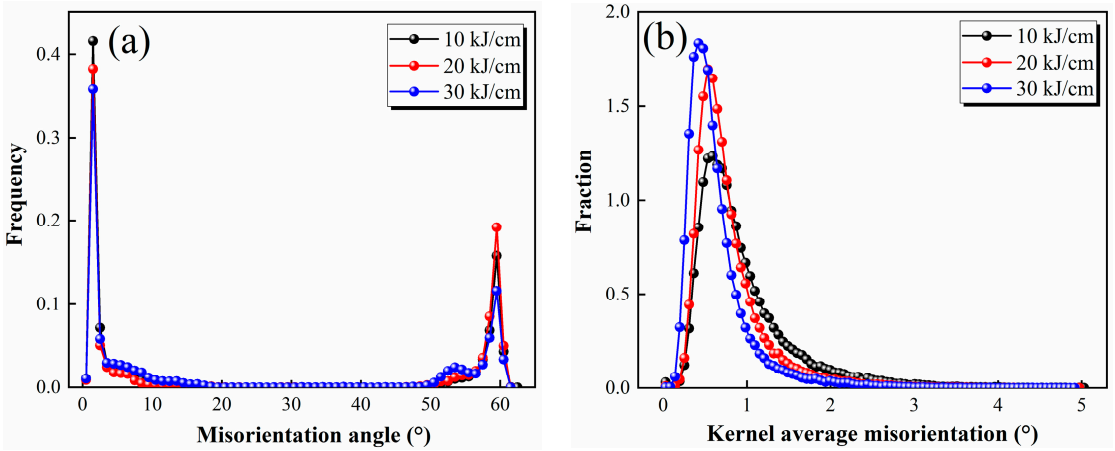

Figure 10. (**a**) Frequency of grain boundaries and (**b**) KAM value evolution in the typical austenite grains in Figure 9.

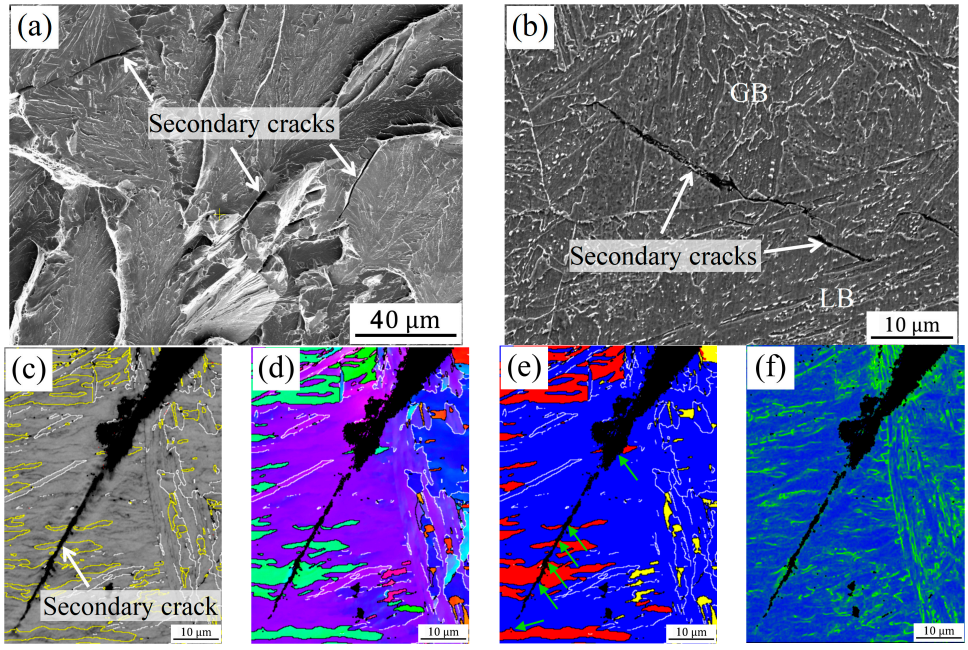

Figure 11. Secondary cracks observed on the fractured V-notch Charpy sample of core with heat input of 30 kJ/cm by using SEM (**a**,**b**) and EBSD (**c**–**f**): (**c**) grain boundary map, (**d**) IPF, (**e**) block map and (**f**) KAM map.

3.5. Overall Discussion

The above results indicate that the inhomogeneous microstructure caused by the segregation of C and Mn in the steel plate not only affects the performance of the matrix, but also passes to the welding zone and has a more serious impact on low-temperature impact toughness. This is because the welding zone is more sensitive to the type of microstructure and stress concentration than the matrix. In addition, the frequent occurrence of "two high and one low" or "two low and one high" phenomena in the impact toughness of high-strength steel should be closely related to the abnormal structure induced by alloy composition segregation. Previous studies [15,26] have shown that it is difficult to eliminate centerline segregation through solid solution treatment and hot rolling. Therefore, for the studied steel, it is necessary to optimize the continuous casting process or reduce the Mn content to eliminate or reduce the degree of segregation, although segregation does not have a significant impact on the matrix properties due to the small thickness of the steel plate. Meanwhile, this study also found that the appropriate welding heat input for 460 MPa grade wind power steel is ~20 kJ/cm. The optimal match through heat input can significantly refine the microstructure of CGHAZ from a crystallographic perspective, which helps to improve the weldability of ultra-high-strength steel.

4. Conclusions

Simulation tests on high-strength wind power steel made by thermo-mechanical controlled processing (TMCP) with yield strength min. 460 MPa and thickness of 20 mm showed that:

(1) Even if the thickness is only 20 mm, the core of wind power steel plates mainly composed of ferrite and pearlite structures will still form a C and Mn segregation band. And the segregation of C and Mn can lead to the formation of martensite and M/A constituent and increase the impact toughness scatter of the matrix.

(2) The centerline segregation of the steel plate can also affect the welding microstructure and properties. Due to the segregation of alloying elements, especially Mn segregation, the tendency for martensite formation in simulated CGHAZ increases, and the hardness of the transformed microstructure is significantly higher than that of the

normal microstructure, which can easily lead to a decrease in impact toughness and an increase in scatter.

(3) For the studied steel with yield strength of ~460 MPa used for wind power generation, there is an optimal welding heat input (~20 kJ/cm), which enables the simulated CGHAZ to obtain the highest impact toughness due to the formation of LB structure and the finest crystallographic block units.

Author Contributions: Writing—original draft preparation, X.W. (Xuelin Wang); investigation and data curation, X.W. (Xiaoya Wang) and W.L.; writing—review and editing, C.S. All authors have read and agreed to the published version of the manuscript.

Funding: This work was funded by the Basic Research and Application Basic Research Foundation of Guangdong Province (No. 2022A1515240016), the National Key Research and Development Project of China (No. 2022YFB3708200), the National Natural Science Foundation of China (No. 52271089) and the Major Scientific and Technological Innovation Project of CITIC Group (No. 2022zxkya06100).

Data Availability Statement: The data presented in this study are available on request from the corresponding author. The data are not publicly available due to privacy.

Acknowledgments: We greatly appreciate Zhongzhu Liu from CITIC Metal Co., Ltd. for his guidance and support on the simulated welding process in this study.

Conflicts of Interest: The authors declare no conflict of interest.

References

1. Zheng, D.D.; Guo, H.C.; Zhang, S.J.; Liu, Y.L. Study on fatigue performance of double cover plate through-core bolted joint of rectangular concrete-filled steel tube bundle wind turbine towers. *J. Constr. Steel Res.* **2023**, *203*, 107830. [CrossRef]
2. Yuan, R.; Pan, Z.D.; Wu, H.B. Effect of normalizing process on microstructure and properties of 420 MPa grade steel plate for offshore wind power. *Heat Treat. Met.* **2021**, *46*, 112–116.
3. Lee, S.; Kim, B.C.; Kwon, D. Correlation of microstructure and fracture properties in weld heat-affected zones of thermomechanically controlled processed steels. *Metall. Mater. Trans. A* **1992**, *23A*, 2803–2816. [CrossRef]
4. Cui, B.; Liu, Z.W.; Liu, Z.; Peng, M.D.; Shi, Q.B.; Cong, J.Q. Effect of welding heat input on microstructural evolution and impact toughness of the simulated coarse-grained heat-affected zone of Q960 steel. *Weld. World* **2023**, *67*, 235–249. [CrossRef]
5. Shao, J.J.; Fei, J.Y.; Zhong, S.F.; Zhao, L.; Xu, L.Y.; Han, Y.D. Microstructure and properties of intercritically reheated coarse-grained heat affected zone in X65 pipeline steel with pre-strain. *Int. J. Hydrogen Energy* **2024**, *49*, 1345–1357. [CrossRef]
6. Lan, L.Y.; Qiu, C.L.; Zhao, D.W.; Gao, X.H.; Du, L.X. Microstructural characteristics and toughness of the simulated coarse grained heat affected zone of high strength low carbon bainitic steel. *Mater. Sci. Eng. A* **2011**, *529*, 192–200. [CrossRef]
7. Moeinifar, S.; Kokabi, A.H.; Madaah Hosseini, H.R. Influence of peak temperature during simulation and real thermal cycles on microstructure and fracture properties of the reheated zones. *Mater. Sci. Eng. A* **2010**, *31*, 2948–2955. [CrossRef]
8. Bertolo, V.; Jiang, Q.; Terol Sanchez, M.; Riemslag, T.; Walters, C.L.; Sietsma, J.; Popovich, V. Cleavage fracture micromechanisms in simulated heat affected zones of S690 high strength steels. *Mater. Sci. Eng. A* **2023**, *868*, 144762. [CrossRef]
9. Shi, Y.W.; Chen, D.; Lei, Y.P.; Li, X.Y. HAZ microstructure simulation in welding of a ultra fine grain steel. *Comput. Mater. Sci.* **2004**, *31*, 379–388. [CrossRef]
10. Yang, Y.L.; Jia, X.; Ma, Y.X.; Wang, P.; Zhu, F.X. Effect of Nb on inclusions and phase transformation in simulated high heat input coarse-grain HAZ of Nb/Ti low carbon microalloyed steel. *Mater. Charact.* **2022**, *189*, 111966. [CrossRef]
11. Sisodia, R.; Weglowski, M.; Sliwinski, P. In situ localised post-weld heat treatment with electron beam welding of S690QL steel. *J. Adv. Join. Process.* **2024**, *9*, 100182. [CrossRef]
12. Zhang, J.; Xin, W.B.; Ge, Z.W.; Luo, G.P.; Peng, J. Effect of high heat input welding on the microstructures, precipitates and mechanical properties in the simulated coarse grained heat affected zone of a low carbon Nb-V-Ti-N microalloyed steel. *Mater. Charact.* **2023**, *199*, 112849. [CrossRef]
13. Liu, Z.P.; Xie, Z.J.; Luo, D.; Zhou, W.H.; Guo, H.; Shang, C.J. Influence of central segregation on the welding microstructure and properties of FH40 cryogenic steel. *Chin. J. Eng.* **2023**, *45*, 1335–1341.
14. Abraham Mathews, J.; Sietsma, J.; Petrov, R.H.; Santofimia, M.J. Influence of chemical segregation on bainitic microstructures in a carburized bearing steel. *Mater. Des.* **2022**, *223*, 111232. [CrossRef]
15. Wang, J.L.; Qian, R.T.; Yang, X.; Zhong, Y.; Shang, C.J. Effect of segregation on the microstructure and properties of a quenching and partitioning steel. *Mater. Lett.* **2022**, *325*, 132815. [CrossRef]
16. Li, W.G.; Zhou, Q.J.; Wu, W.J.; Tong, Y.X.; Li, J.X. Effect of the segregation band on the hydrogen embrittlement susceptibility of quenched and partitioned steel. *Corros. Sci.* **2023**, *22*, 111436. [CrossRef]

17. Han, P.; Liu, Z.P.; Xie, Z.J.; Wang, H.; Jin, Y.H.; Wang, X.L.; Shang, C.J. Influence of band microstructure on carbide precipitation behavior and toughness of 1 GPa-grade ultra-heavy gauge low-alloy steel. *Int. J. Miner. Metall. Mater.* **2023**, *30*, 1329–1337. [CrossRef]
18. Shi, L.; Long, J.; Pang, H.Y.; Lin, M.X.; Zhang, H.J.; Wu, T. Study on microstructure and low temperature impact toughness of large thickness steel for offshore wind power. *J. Chongqing Univ.* **2023**, 1–9. Available online: https://link.cnki.net/urlid/50.1044.n.20231120.2011.002 (accessed on 21 November 2023).
19. Kitahara, H.; Ueji, R.; Tsuji, N.; Minamino, Y. Crystallographic features of lath martensite in low-carbon steel. *Acta Mater.* **2006**, *54*, 1279–1288. [CrossRef]
20. Lambert-Perlade, A.; Sturel, T.; Gourgues, A.F.; Besson, J.; Pineau, A. Mechanisms and modeling of cleavage fracture in simulated heat-affected zone microstructures of a high-strength low alloy steel. *Metall. Mater. Trans. A* **2004**, *35*, 1039–1053. [CrossRef]
21. *E8/E8M-16a*; Standard Test Methods for Tension Testing of Metallic Materials. ASTM: West Conshohocken, PA, USA, 2016.
22. *E384-9*; Standard Test Method for Microindentation Hardness of Materials. ASTM: West Conshohocken, PA, USA, 2009.
23. Zhang, N.Z.; Zhao, H.T.; Zhou, F.; Chen, X.M.; Bao, L.J.; Shi, G. Mechanical properties and constitutive model of Q345GJ thick steel plate in China. *Constr. Build. Mater.* **2023**, *406*, 133288. [CrossRef]
24. *GB/T 1591-2018*; High Strength Low Alloy Structural Steels. China Iron and Steel Association: Beijing, China, 2018.
25. Domizzi, G.; Anteri, G.; Ovejero-Garcıa, J. Influence of sulphur content and inclusion distribution on the hydrogen induced blister cracking in pressure vessel and pipeline steels. *Corros. Sci.* **2001**, *43*, 325–339. [CrossRef]
26. Xie, Z.J.; Li, Q.; Liu, Z.P.; Zhou, W.J.; Wang, X.L.; Yu, Q.; Xiao, D.H.; Shang, C.J. Enhanced ductility and toughness by tailoring heterogenous microstructure in an ultra-heavy gauge high strength steel with severe centerline segregation. *Mater. Lett.* **2022**, *323*, 132525. [CrossRef]
27. Yang, X.C.; Di, X.J.; Liu, X.G.; Wang, D.P.; Li, C.N. Effects of heat input on microstructure and fracture toughness of simulated coarse-grained heat affected zone for HSLA steels. *Mater. Charact.* **2019**, *155*, 109818. [CrossRef]
28. Gou, J.X.; Xing, X.; Cui, G.; Li, Z.L.; Liu, J.G.; Deng, X.Y.; Cheng, Y.F. Effect of hydrogen on impact fracture of X80 steel weld: Various heat inputs and coarse grain heat-affected zone. *Mater. Sci. Eng. A* **2023**, *886*, 145673. [CrossRef]
29. Wang, X.L.; Su, W.J.; Xie, Z.J.; Li, X.C.; Zhou, W.H.; Shang, C.J.; Wang, Q.C.; Bai, J.; Wu, L.Q. Microstructure evolution of heat-afected zone in submerged arc welding and laser hybrid welding of 690 MPa high strength steel and its relationship with ductile-brittle transition temperature. *Acta Metall. Sin. Engl. Lett.* **2023**, *36*, 623–636. [CrossRef]
30. Takayama, N.; Miyamoto, G.; Furuhara, T. Effects of transformation temperature on variant pairing of bainitic ferrite in low carbon steel. *Acta Mater.* **2012**, *60*, 2387–2396. [CrossRef]
31. Morito, S.; Huang, X.; Furuhara, T.; Maki, T.; Hansen, N. The morphology and crystallography of lath martensite in alloy steels. *Acta Mater.* **2006**, *54*, 5323–5331. [CrossRef]
32. Qi, X.N.; Huan, P.C.; Wang, X.N.; Di, H.S.; Shen, X.J.; Sun, Q.; Liu, Z.G.; He, J.R. Study on the mechanism of heat input on the grain boundary distribution and impact toughness in CGHAZ of X100 pipeline steel from the aspect of variant. *Mater. Charact.* **2021**, *179*, 111344. [CrossRef]
33. Terasaki, H.; Shintome, Y.; Komizo, Y.I.; Ohata, M.; Moriguchi, K.; Tomio, Y. Effect of close-packed plane boundaries in a Bain zone on the crack path in simulated coarsegrained HAZ of bainitic steel. *Metall. Mater. Trans. A* **2015**, *46*, 2035–2039. [CrossRef]
34. Gourgues, A.F. Electron backscatter diffraction and cracking. *Mater. Sci. Technol.* **2012**, *18*, 119–133. [CrossRef]
35. Chakrabarti, D.; Strangwood, M.; Davis, C.L. Effect of bimodal grain size distribution on scatter in toughness. *Metall. Mater. Trans. A* **2009**, *40*, 780–795. [CrossRef]
36. Kang, S.; Speer, J.G.; Regier, R.W.; Nako, H.; Kennett, S.C.; Findley, K.O. The analysis of bainitic ferrite microstructure in microalloyed plate steels through quantitative characterization of intervariant boundarie. *Mater. Sci. Eng. A* **2016**, *669*, 459–468. [CrossRef]
37. Furuhara, T.; Takayama, N.; Miyamoto, G. Key factors in grain refinement of martensite and bainite. *Mater. Sci. Forum* **2010**, *638*, 3044–3049. [CrossRef]